Signal-to-Noise Ratio Analysis of a Phase-Sensitive Voltmeter for Electrical Impedance Tomography

Ethan K. Murphy*, Mohammad Takhti*, Joseph Skinner, Ryan J. Halter, and Kofi Odame

***Abstract*—In this paper, thorough analysis along with mathematical derivations of the matched filter for a voltmeter used in electrical impedance tomography systems are presented. The effect of the random noise in the system prior to the matched filter, generated by other components, are considered. Employing the presented equations allow system/circuit designers to find the maximum tolerable noise prior to the matched filter that leads to the target signal-to-noise ratio (SNR) of the voltmeter, without having to over-design internal components. A practical model was developed that should fall within 2 dB and 5 dB of the median SNR measurements of signal amplitude and phase, respectively. In order to validate our claims, simulation and experimental measurements have been performed with an analog-to-digital converter (ADC) followed by a digital matched filter, while the noise of the whole system was modeled as the input referred at the ADC input. The input signal was contaminated by a known value of additive white Gaussian noise (AWGN) noise, and the noise level was swept from 3% to 75% of the least significant bit (LSB) of the ADC. Differences between experimental and both simulated and analytical SNR values were less than 0.59 and 0.35 dB for RMS values $\geq$20% of an LSB and less than 1.45 and 2.58 dB for RMS values $<$20% of an LSB for the amplitude and phase, respectively. Overall, this study provides a practical model for circuit designers in EIT, and a more accurate error analysis that was previously missing in EIT literature.**

***Index Terms*—Electrical impedance imaging, matched filter, digital voltmeter, random noise, mathematical derivations, ADC.**

I. Introduction

IMAGE reconstruction in electrical impedance tomography (EIT) aims to estimate the spatially varying electrical properties within a domain from a set of boundary voltage measurements. The amplitudes and phases of these measurements carry information about the internal electrical properties, and by processing them, it is possible to estimate the spatial distribution of conductivity and permittivity. Recently, EIT has been considered in a number of medical applications, and it is attractive due to its affordability, its safe non-ionizing radiation-based nature [1], and its potential for portability and miniaturization [2], [3], [4]. A positive trend towards EITs acceptance in medical imaging is the release of several commercial systems for lung ventilation and perfusion monitoring applications [5].

One challenge with EIT is that the image reconstruction problem is poorly conditioned and ill-posed, meaning that the boundary voltage measurements must be read out at signal-to-noise ratios (SNRs) as high as 90 dB [6]. Insufficiently high SNR makes the different impedance distributions indistinguishable from each other, resulting in EIT images that are of limited clinical value. Ordinarily, these SNR levels have challenging power and area implications for the circuit integration of a multi-channel, multi-MHz signal application such as EIT.

Fortunately, the EIT readout chain incorporates a matched filter, which makes high SNR achievable even with relatively low-precision circuit components [7], [8], [9]. For instance, depending on electronic circuit noise levels and the number of taps in the matched filter, a 10 bit resolution analog-to-digital converter (ADC) is sufficient for 96 dB SNR. Previous investigators (e.g. [9], [10]) have recognized this possibility, but their results do not completely take into account how electronic noise and quantization error will interact to affect SNR. Further, previous work has rarely considered the SNR of phase measurements, focusing only on amplitude. It is difficult for the circuit designer to use these previous results to make proper trade-offs and decisions between various circuit specifications to try to meet EIT performance goals. Although EIT relies on in-phase and quadrature (or real and reactive) components for performing reconstructions, we concern ourselves here with analyzing the SNR of the amplitude and phase because these are important for analyzing system performance ([11]) and in calibrating an EIT system ([6], [12]).

In this paper, we formulate the SNR of both the extracted amplitude and phase of the matched filter considering both quantization and additive electronic noise of the system. An analytic and two approximate models are developed. The approximate models are referred to as the Discrete Uniform (DU) and Continuous Uniform (CU) models. Based on simulations (validated through measurements), the DU model should fall within 2 dB and 5 dB of the median SNR measurements of signal amplitude and phase, respectively, and the CU model should fall within 6.5 dB and 11 dB of the median SNR measurements of signal amplitude and phase, respectively. Thus a circuit designer could use the, more accurate, DU model to translate a target SNR to circuit-level specifications that incorporate various parameters including electronic noise budget, ADC resolution, and number of filter taps of the matched filter. Therefore, the designer can budget the noise between different blocks prior to the matched filter, without having to over-design the system.

Determining SNR in terms of circuit-level specification is not unique to EIT; numerous works have studied closely related problems. Quantization noise due to an ADC has

Manuscript received XX, 2015. This work was supported in part by the U.S. National Science Foundation (NSF) under Grant Number IIS-1418497. Asterisk indicates corresponding authors.

*Ethan K. Murphy, *Mohammad Takhti, Ryan Halter, and Kofi Odame are with the Thayer School of Engineering, 14 Engineering Drive, Dartmouth College, Hanover, NH 03755 USA, (e-mail:ethan.k.murphy@dartmouth.edu, mohammad.takhti@dartmouth.edu).

been thoroughly explored beginning around 1947 [13], [14]. Error propagation of noisy signals through an ADC has been considered in the area of signal processing [15], where it is referred to as non-subtractive dither. In [15], a simple expression, which corresponds to our Continuous Uniform (CU) model, is described and analyzed for when it is technically applicable. As they considered dither, noise produced from a user-specified probability distribution, their results are not directly applicable in the case of Gaussian additive noise. Error modeling and analysis of digital matched filters is also well-studied in signal-processing literature, e.g. [16], but our particular signal, additive noise (distribution and range), ADC, and matched filter appear to have not been considered.

The remainder of this paper is organized as follows; Section II describes amplitude and phase extraction using a matched filter, Section III discusses the noise resulting from analog and mixed-signal circuits, Section IV presents the analytic expressions for the SNR, and Section V discusses the DU model and its utility. The analytic model and our simulation code are validated by a set of measured data (Section IV.B), and two sets of example curves produced by the DU model illustrate how the model can aid in circuit design (Section V). Although the analytic model is very accurate, it would be unpractical to use prior to circuit construction. However, the DU model provides a real practical SNR formula that could help circuit designers achieve an SNR tolerance. Overall, the DU model yields a specific and accurate SNR formulation that provides a practical use and error description that was missing in the EIT literature.

II. Amplitude and Phase Extraction

In EIT, a low-amplitude sinusoidal current of frequency f Hz is injected into the tissue via a pair of electrodes. This injected current results in a set of boundary voltages developing across the surface of the tissue, each of which is measured with phase-sensitive voltage readout circuitry. The readout circuit provides both amplitude (A) and phase (ϕ) information, based on the in-phase and quadrature ('I' and 'Q') components of the time-dependent boundary voltage, $V_{\mathrm{BND}}(t)$:

$$\begin{aligned} V_{\mathrm{BND}}(t) &= A\sin(2\pi ft+\phi) \\ &= \underbrace{A\cos(\phi)}_{\mathrm{V_I}}\sin(2\pi ft) + \underbrace{A\sin(\phi)}_{\mathrm{V_Q}}\cos(2\pi ft). \end{aligned} \quad (1)$$

The I/Q components, V_{I} and V_{Q}, can be extracted by multiplying the boundary voltage with orthogonal sinusoidal signals and integrating over one period, $T = 1/f$. This yields

$$V_{\mathrm{I}} = \frac{2}{T}\int_0^T V_{\mathrm{BND}}(t)\sin(2\pi ft) = A\cos(\phi) \quad (2)$$

and

$$V_{\mathrm{Q}} = \frac{2}{T}\int_0^T V_{\mathrm{BND}}(t)\cos(2\pi ft) = A\sin(\phi). \quad (3)$$

In general, more than one period can be sampled; through averaging this can increase the SNR of the measurements. From the I/Q components, the amplitude and phase of the boundary voltage can be calculated as

$$A = \sqrt{V_{\mathrm{Q}}^2 + V_{\mathrm{I}}^2}, \quad (4)$$

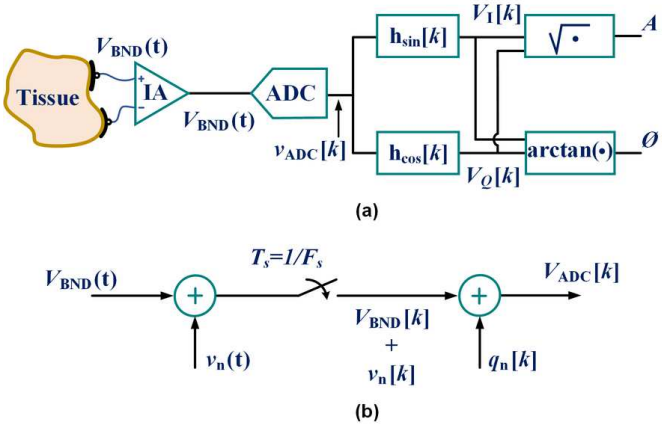

Fig. 1. (a) Simplified block diagram of a typical EIT readout channel, and (b) detail of the signal processing chain from the instrumentation amplifier (IA) input to the ADC output. The boundary voltage $V_{BND}(t)$ is corrupted by electrical noise, $v_{\mathrm{n}}(t)$. This noisy signal is sampled by the ADC at a rate of F_{s}. Finally, the sampled signal is converted to the digital value $V_{ADC}[k]$, by adding a quantization noise term, $q_{\mathrm{n}}[k]$.

and

$$\phi = \arctan\left(\frac{V_{\mathrm{Q}}}{V_{\mathrm{I}}}\right). \quad (5)$$

Any errors in the readout circuit will affect how precisely we can measure these amplitude and phase values. In turn, measurement precision is a major factor in determining the imaging quality of the EIT system as a whole. The remainder of this paper will explore the relationship between circuit-level error and overall measurement precision. Practically, this is explored by finding the SNR of the output signal. The primary effort is in the calculation of the (variance of the) noise.

III. Noise from Analog and Mixed-Signal Circuits

Fig. 1 (a) is a simplified diagram of a typical EIT readout circuit. The boundary voltage, V_{BND}, is sensed on a pair of electrodes and amplified by an instrumentation amplifier. The amplified voltage is then converted to a digital signal with an ADC. A pair of digital filters perform the I/Q extraction and additional processing calculates the amplitude and phase of the signal.

The instrumentation amplifier and the analog components of the ADC both produce random electronic noise from their component devices. The noise from all of these sources can be lumped together and modeled as a single additive white Gaussian noise (AWGN) voltage signal, $v_{\mathrm{n}}(t)$, that is referred to the input of the ADC (see Fig. 1 (b)). This is a common assumption. The flicker noise and the corner frequency vary from design to design, since it is device and design dependent, and can be lowered by proper design and circuit techniques [17]. The 1/f corner frequency reported for commercial amplifiers shows the corner frequency as low as 500 Hz for CMOS amplifiers [18]. In EIT, 1/f noise can be likely ignored based on the moderately high current frequencies (1 kHz - 10 MHz). It is common to assume that electronic noise (assumed predominately to be from thermal sources) is AWGN [19], and the practice of combining different noise sources into a single

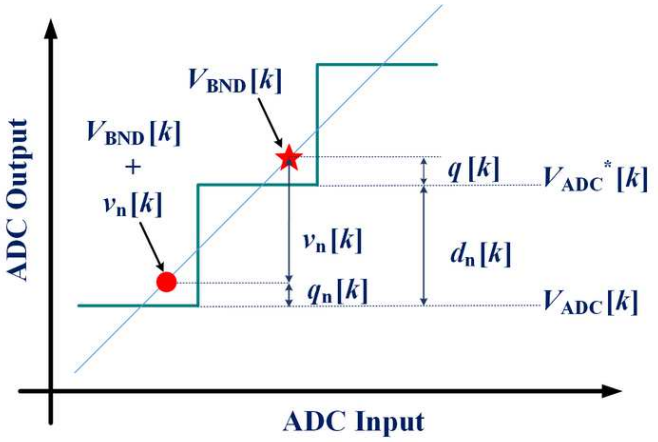

Fig. 2. Illustration of the two equivalent descriptions of the random system and quantization (ADC) noise. The ADC output is $V_{ADC}[k]$, which is a quantized version of the sampled noisy input, $V_{BND}[k]+v_{\rm n}[k]$. If the ADC input were clean, then its output would be $V^*_{ADC}[k]$, which is a quantized version of $V_{BND}[k]$. The difference between this theoretical, clean ADC output and the actual (noisy) ADC output is the discrete noise term, $d_{\rm n}[k]$. So, $V_{ADC}[k]$ can also be written as the sum of $d_{\rm n}[k]$ and $V^*_{ADC}[k]$.

term is a standard approach [19], [20]. We note that noise due to current or tissue sources are not explicitly considered in this study.

The AWGN noise is added to the otherwise clean signal, $V_{\rm BND}(t)$, and sampled by the ADC to produce $V_{\rm BND}[k]+v_{\rm n}[k]$, where k is a discrete time index. The ADC then quantizes the sampled signal, which is equivalent to adding quantization noise, $q_{\rm n}[k]$, to the signal. Thus, the output of the ADC can be written as

$$V_{\rm ADC}[k] = V_{\rm BND}[k] + q_{\rm n}[k] + v_{\rm n}[k], \tag{6}$$

where $v_{\rm n}[k]$ and $q_{\rm n}[k]$ are both continuous valued, random variables, with $q_{\rm n}[k]$ dependent on $V_{\rm BND}[k]$ and $v_{\rm n}[k]$.

Fig. 2 presents an equivalent, perhaps more tractable model of the k'th ADC output. In this model, we can think of the ADC output as the sampled clean input plus two error terms:

$$V_{\rm ADC}[k] = V_{\rm BND}[k] + q[k] + d_{\rm n}[k]. \tag{7}$$

Here, $q[k]$ is a quantization error that is completely deterministic; it is the difference between the clean input sample, $V_{\rm BND}[k]$ and the closest ADC quantization level, $V^*_{ADC}[k]$ from Fig. 2. The second error term, $d_{\rm n}[k]$ is a discrete-valued random variable of the form mLSB, where m is an integer and LSB is the least significant bit. The LSB for a b-bit ADC is defined by LSB $= V_{FS}/2^b$, where V_{FS} is the full-scale voltage. For a derivation of (7) see Appendix A.

The main advantage of expressing $V_{\rm ADC}[k]$ with Eq. (7) is that it expresses the error as a single random variable, $d_{\rm n}$, as opposed to two correlated random variables ($q_{\rm n}[k]$ and $v_{\rm n}[k]$ in Eq. (6)). This means that the amount of noise in $V_{\rm ADC}[k]$ is simply given by the variance of $d_{\rm n}[k]$, i.e.

$$\begin{aligned}\mathrm{var}(V_{\rm ADC}[k]) &= \mathrm{var}(d_{\rm n}[k]) \\ &= \textstyle\sum_{m=-\infty}^{\infty} P(d_{\rm n}[k] = m\mathrm{LSB})(m\mathrm{LSB} - E[d_{\rm n}[k]])^2,\end{aligned} \tag{8}$$

where $E[d_{\rm n}[k]]$ is the expected value of $d_{\rm n}[k]$, and $P(d_{\rm n}[k] = m\mathrm{LSB})$ is the probability that $d_{\rm n}[k]$ is equal to mLSB. We note that (8) is the definition of variance for a discrete random variable [21]. Since q[k] is deterministic it has a variance of zero, and therefore does not contributed to $\mathrm{var}(V_{\rm ADC}[k])$.

Studying Fig. 2, we see that $d_{\rm n}[k]$ is a discretization of the random and quantization error. We assume the random error ($v_{\rm n}[k]$) to be normally distributed with a standard deviation of σ_n. Incorporating the deterministic error $q[k]$ into the random error ($v_{\rm n}[k]$) is equivalent to offsetting its mean by $q[k]$. Thus the probability of $d_{\rm n}[k]$ attaining a given value mLSB is determined by evaluating the probability of the normal error ($v_{\rm n}[k]$) offset by the quantization error $q[k]$ being within the interval $[(m-0.5)\mathrm{LSB}, (m+0.5)\mathrm{LSB}]$, i.e. $P(d_{\rm n}[k] = m\mathrm{LSB})$ is given by

$$\begin{aligned}&P(d_{\rm n}[k] = m\mathrm{LSB}) = \\ &= P((m-0.5)\mathrm{LSB} < v_{\rm n}[k] - q[k] < (m+0.5)\mathrm{LSB}) \\ &= \tfrac{1}{\sigma_{\rm n}\sqrt{2\pi}} \textstyle\int_{(m-0.5)\mathrm{LSB}}^{(m+0.5)\mathrm{LSB}} \exp\left(\frac{-(x-q[k])^2}{2\sigma_{\rm n}^2}\right) dx,\end{aligned} \tag{9}$$

where the variable x in the integral represents the random normal error $v_n[k]$, and the last line of (9) follows from the previous line by definition ([21]) given that $v_n[k]$ is an AWGN with standard deviation σ_n.

Fig. 3 provides an additional illustration of how the error is modeled. It shows the continuous probability distribution function (pdf) of the input random error, $v_{\rm n}[k]$, offset by the deterministic error, $q[k]$, and the resulting discrete probability mass function (pmf) that represents the distribution of the output random error, $d_{\rm n}[k]$, of the ADC. This illustrates the dependence of $d_{\rm n}[k]$ on the width of the normal error and the offset location due to the deterministic error.

IV. Signal-to-noise Ratio in a Phase-Sensitive Measurement System

To predict the SNR that we can expect from the readout circuit, we will consider the noise signal, $d_{\rm n}[k]$, and how it propagates through the I/Q extraction to the final amplitude and phase measurements.

The SNR of the amplitude and phase of the whole chain shown in Fig. 1 can be found using the following:

$$SNR_{A\backslash\phi} = 10\log_{10}\frac{(\bar{V}^2_{A\backslash\phi})}{\mathrm{var}(A\backslash\phi)} \tag{10}$$

where $\bar{V}_{A\backslash\phi}$ and $\mathrm{var}(A\backslash\phi)$ are the mean and variance, respectively, of the amplitude and phase. In the remainder of this section, equations for the amplitude and phase SNRs will be defined by finding the mean and variance of the amplitude and phase, and these equations are compared to the SNR from a set of measured data. In order to find the aforementioned mean and variance values, one needs to first calculate the mean and variance of the in-phase and quadrature components.

A. SNR using the Analytical Model

Fig. 1 showed the I/Q extraction being performed in the digital domain; implementing the I/Q extraction in its original

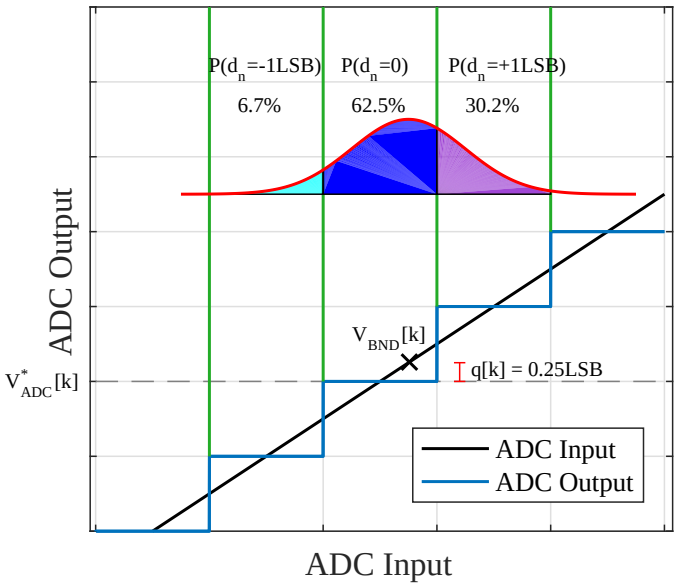

Fig. 3. Illustration of the effect that the random noise, $v_{\rm n}[k]$, has on the ADC output. In this example, the signal $V_{BND}[k]$ should ideally result in an output of $V^*_{ADC}[k]$, which is 0.25 LSB away and is the closest ADC quantization level. However, the presence of the random noise term, $v_{\rm n}[k]$, can cause the ADC output to "jump" by some multiple of an LSB away from the ideal clean output. The probability of a +1 LSB jump is 30.2%, and the probability of a -1 LSB jump is 6.7%. Also, it is possible (62.5% probability) that there will be no jump at all, and that the random noise term has no effect, ultimately, on the ADC output. The random noise $v_{\rm n}[k]$ is assumed to have a normal distribution with zero mean and a standard deviation of 0.5 an LSB.

continuous-time form (Eqs. (2) and (3)) would require costly, high-precision analog components. Instead, low cost, digital matched filters are used to approximate $V_{\rm I}$ and $V_{\rm Q}$ via

$$V_{\rm I} = \frac{2}{N}\sum_{k=0}^{N-1} V_{\rm ADC}[k]\cdot\sin\left(\frac{2\pi f k}{F_{\rm s}}\right) \tag{11}$$

and

$$V_{\rm Q} = \frac{2}{N}\sum_{k=0}^{N-1} V_{\rm ADC}[k]\cdot\cos\left(\frac{2\pi f k}{F_{\rm s}}\right), \tag{12}$$

where $F_{\rm s}$ is the ADC sample rate and N is the number of sample points in one period of the input signal, i.e. for this situation N is also the number of matched filter taps. The amount of noise in the calculated $V_{\rm I}$ and $V_{\rm Q}$ signals is given by

$$\mathrm{var}(V_{\rm I}) = \frac{4}{N^2}\sum_{k=0}^{N-1} \mathrm{var}(d_{\rm n}[k])\cdot\sin^2\left(\frac{2\pi f k}{F_{\rm s}}\right) \tag{13}$$

and

$$\mathrm{var}(V_{\rm Q}) = \frac{4}{N^2}\sum_{k=0}^{N-1} \mathrm{var}(d_{\rm n}[k])\cdot\cos^2\left(\frac{2\pi f k}{F_{\rm s}}\right). \tag{14}$$

Here, we have used the fact (Eq. (8)) that $\mathrm{var}(V_{\rm ADC}[k]) = \mathrm{var}(d_{\rm n}[k])$ and the assumption that the variances, $d_{\rm n}[k]$, are uncorrelated (white).

Recalling Eq. (4), the variance of the amplitude is

$$\begin{aligned}\mathrm{var}(A) &= \mathrm{var}\left(\sqrt{V_{\rm Q}^2+V_{\rm I}^2}\right)\\ &\approx \mathrm{var}(V_{\rm I})\cos^2(\phi)+\mathrm{var}(V_{\rm Q})\sin^2(\phi)\\ &\quad +2\mathrm{cov}(V_{\rm I},V_{\rm Q})\cos(\phi)\sin(\phi)\,,\end{aligned} \tag{15}$$

where we have linearized the function $\sqrt{x^2+y^2}$, on the assumption that the in-phase and quadrature noise is sufficiently small. Appendix B shows the details of our derivation. Similarly, using Eq. (5), we write the variance of the phase as

$$\begin{aligned}\mathrm{var}(\phi) &= \mathrm{var}\left(\arctan\left(\frac{V_{\rm Q}}{V_{\rm I}}\right)\right)\\ &\approx \frac{1}{A^2}\left(\mathrm{var}(V_{\rm I})\sin^2(\phi)+\mathrm{var}(V_{\rm Q})\cos^2(\phi)\right.\\ &\quad \left.-2\mathrm{cov}(V_{\rm I},V_{\rm Q})\cos(\phi)\sin(\phi)\right),\end{aligned} \tag{16}$$

Here, too, we have used a linearization approach to arrive at a simple expression (see Appendix C for details). Further, details of the calculation of the covariance ($\mathrm{cov}(V_{\rm I},V_{\rm Q})$) are given in Appendix D.

From Eqs. (15) and (16), the SNR for the amplitude and phase using Eq. (10) are therefore

$$\begin{aligned}SNR_A = \;& 10\log_{10}(A^2) - 10\log_{10}\left[\mathrm{var}(V_{\rm I})\cos^2\phi\right.\\ &\left.+\mathrm{var}(V_{\rm Q})\sin^2\phi+2\mathrm{cov}(V_{\rm I},V_{\rm Q})\cos(\phi)\sin(\phi)\right],\end{aligned} \tag{17}$$

and

$$\begin{aligned}SNR_\phi = \;& 10\log_{10}(\phi^2A^2) - 10\log_{10}\left[\mathrm{var}(V_{\rm I})\sin^2\phi\right.\\ &\left.+\mathrm{var}(V_{\rm Q})\cos^2\phi-2\mathrm{cov}(V_{\rm I},V_{\rm Q})\cos(\phi)\sin(\phi)\right].\end{aligned} \tag{18}$$

Equations (17) and (18) are purely analytical models to predict the SNR of the amplitude and phase measurements. The model depends on the amount of electronic noise, the ADC resolution, the number of matched filter taps, and the phase of the measured voltage. Therefore, if we wanted to characterize the SNR performance of an EIT system, then we could use this model as a reasonably accurate check against experimental measurement results.

B. Comparison to Measured Data

Fig. 4 are the results of comparing the analytical models, (17) and (18), to measured and simulated data. The DU and CU Models, discussed in detail in the following section, are also included in Fig. 4 for comparison. The measured and simulated SNR values are determined by calculating the mean and standard deviation values of amplitude and phase using (10). The measurement setup involved an evaluation board with an Analog Devices AD7760 24-bit sigma delta ADC, which was chosen to guarantee that the ADC has a very low-level thermal noise ($< 0.38\mu V_{\rm rms}$), much lower than the noise input by the signal generator. A signal generator (Agilent 33522A) input a sinusoidal signal with a frequency of 3.125 kHz (f) and a full-scale voltage, V_{FS} of 6.42 V.

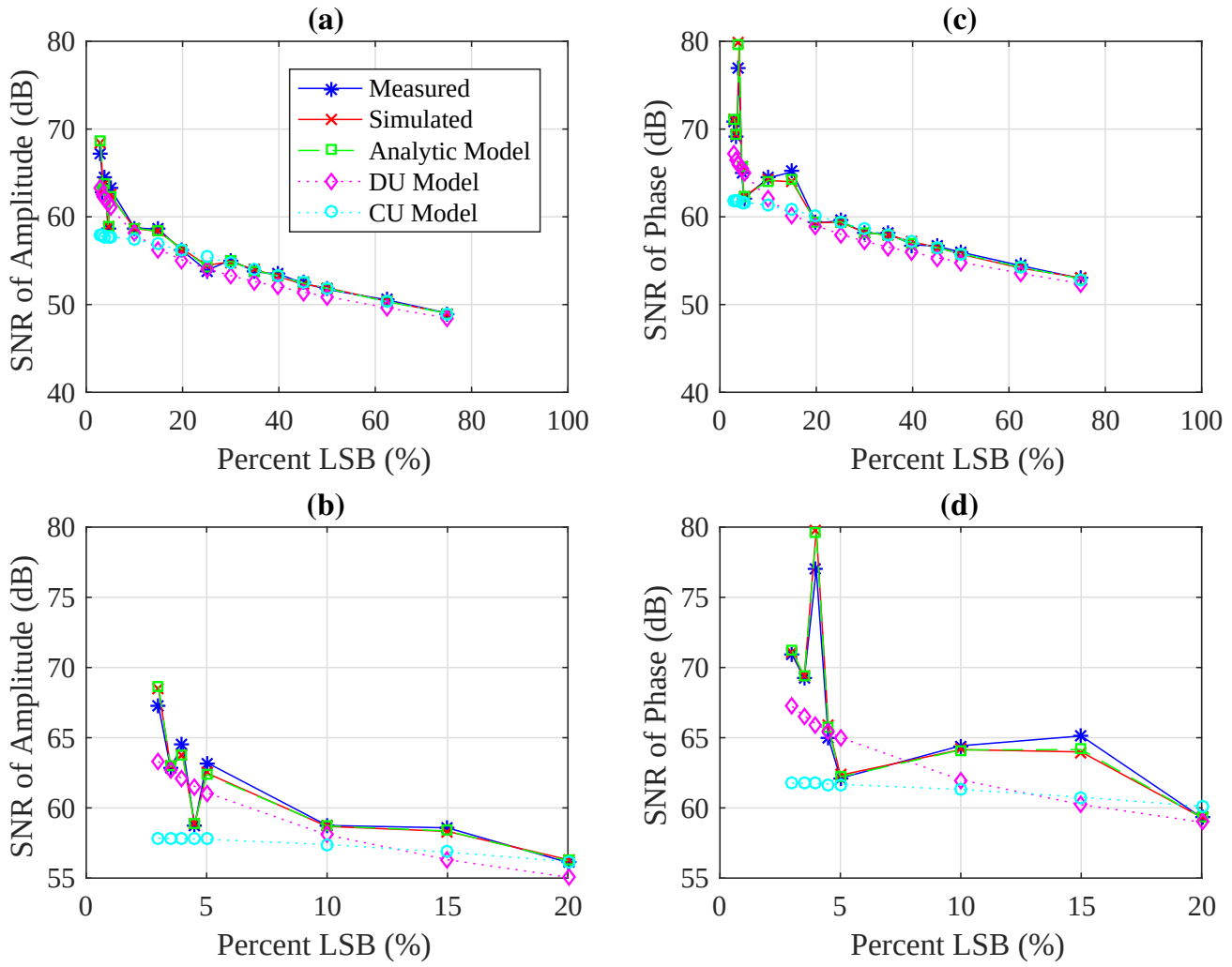

Fig. 4. Comparison of amplitude and phase SNR versus RMS for measured data, simulated data, and the analytic, DU, and CU models. (a) and (c) show ranges from 3-100%, whereas (b) and (d) zooms in on the range of 3-20%.

The effective sampling frequency was 78.125 kHz (F_S) based on the sampling frequency of 20 MHz and a decimation rate of 256 on the evaluation board. This results in 25 equally spaced points per period (N). A total of 5,000 periods were sampled for each measurement set, i.e. these were used to numerically calculate the mean and variance in (10). White Gaussian noise was added to the signal with RMS values (σ_n) ranging from 0.5% to 75% of a 7-bit LSB using the same signal generator. The measurements were reduced to 7-bit values using a straightforward reduction in bit depth using Matlab. We focus on the percent LSB of white noise error, because this is the most significant factor in how the error distribution varies. The minimum noise added to the signal corresponded to 0.5% an LSB or 0.251 mVrms, where the LSB is given by $50.156 \text{ mV} = 6.42/2^7$ V. In order to produce 0.5% LSB increments the signal generator added noise in minimum increments of 1.154 mVrms with a bandwidth of 2.048 MHz, and a low-pass filter was used to remove noise above 64.0591 kHz. Thus reducing in-bandwidth noise. An antialiasing filter on the evaluation board of the ADC, which had a cut-off frequency of 6.97 MHz, was also used. This prevented possible folding of the noise. The simulated data was constructed in Matlab using a 7-bit sinusoidal signal with the same frequency, sampling frequency, number of samples, and added noise as the measured data.

In Fig. 4 one can see very good agreement for RMS values 20% of an LSB and higher. Specifically, maximum absolute differences between all combinations of analytic, simulated, and measured data is less than 0.59 dB and 0.35 dB for amplitude and phase measurements, respectively. For RMS values less than 20% an LSB the differences between measured and analytic data (or simulated) increases, but are less than 1.45 and 2.58 dB for amplitude and phase, respectively. The differences between simulated and analytic SNR values are less than 0.25 dB over all RMS values. The non-smooth aspects of the curves at low RMS values are due to different phase values (i.e. different deterministic quantization errors across different RMS values), which was due to the fact that the phase of the input signal was not explicitly set. Small deviations between measured and simulated (or the analytic model) appear due to phase drifts and DC offsets in the data that could not be entirely removed.

V. Determining Circuit-Level Specifications to Meet a SNR Target

Beyond its use to verify measurement results, the model of Eqs. (17) and (18) would be a powerful design tool, if, given a target SNR, it could provide a corresponding set of required circuit design specifications (e.g. noise budget, ADC resolution, number of filter taps) that must be met. Unfortunately, Eqs. (17) and (18) are unhelpful in this regard, because they are based on Eq. (9), which depends on the phase of a boundary voltage that will be known only *after* the circuit has been designed and deployed in a functioning EIT system.

Even though the individual sample values are unknown during circuit design, we do have an idea about their statistics. In particular, we know that the quantization error resembles a random variable with a uniform distribution between -0.5LSB and 0.5LSB. We refer to this as the Discrete Uniform (DU) model. Using this assumption, we can recalculate the probability function (9) giving us

$$P(d_{\mathrm{n}}^{DU} = m\mathrm{LSB}) = \frac{1}{LSB}\int_{-LSB/2}^{+LSB/2}\frac{1}{\sigma_{\mathrm{n}}\sqrt{2\pi}}\times \int_{(m-0.5)\mathrm{LSB}}^{(m+0.5)\mathrm{LSB}}\exp\left(\frac{-(x-z)^2}{2\sigma_{\mathrm{n}}^2}\right)dxdz, \tag{19}$$

where we have averaged (integrated) over all possible $q[k]$ values, which also has the effect of removing the dependence on k. In (19), z is associated with $q[k]$ and x is associated with $v_{\mathrm{n}}[k]$. Next, one can calculate the variance of the error in the DU model, $\mathrm{var}(d_{\mathrm{n}}^{DU})$ similarly to (8). Since there is no longer a k dependence, (13) and (14) simplify to

$$\mathrm{var}(V_{I/Q}^{DU}) = 2/N \times \mathrm{var}(d_{\mathrm{n}}^{DU}), \tag{20}$$

and the covariance term, $cov(V_I, V_Q)$, is zero. The covariance is zero because once the d_n terms can be pulled out of the summations in (A.21) and (A.24) the sine and cosine terms sum to zero. Thus the SNR equations of the DU model are given by

$$SNR_A^{DU} = 10\log_{10}\frac{A^2(N/2)}{\mathrm{var}(d_{\mathrm{n}}^{DU})}, \tag{21}$$

and

$$SNR_\phi^{DU} = 10\log_{10}\frac{\phi^2(A^2N/2)}{\mathrm{var}(d_{\mathrm{n}}^{DU})}. \tag{22}$$

Given a particular set of design parameters, the DU model of (21) and (22) is able to predict a reasonably representative value for SNR (Figs. 4 and 5). The actual SNR might vary over a wide range, but in practice (and in our simulated experiments) it is expected to fall within ± 2 dB of the median value; the DU model provides an estimated SNR that is within this window (see Fig. 6). As the SNR can vary due to the phase of the signal, this bound was determined by investigating simulations of SNR based on 5,000 phase values uniformly ranging from 0 to 90 degrees with all other parameters taken to be the same as the measured scenario (Section IV.B). Therefore, a circuit designer can use this model to translate a target SNR to circuit-level specifications. Fig. 7 illustrates two sets of curves that show the various combinations of electronic noise budget (RMS), ADC resolution and number of filter taps (N) that could be used to achieve an SNR of 80 dB.

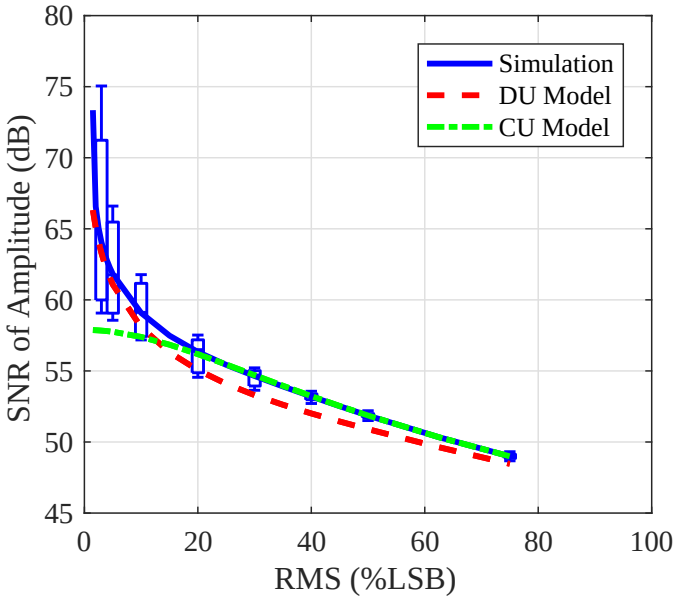

Fig. 5. Illustration of the SNR amplitude corresponding to the DU and CU models and calculated from 5,000 simulated noisy input signals which uniformly vary phase from 0 to 90 degrees with RMS values ranging from 3-75% an LSB. The input signal assumes the same scenario as the measured scenario (Fig. 4).

Specifically, Fig. 7 (a) compares an 8-, 10-, and 12-bit ADC with $N = 25$, and, Fig. 7 (b) compares 10, 100, and 1,000 filter taps for a 10-bit ADC. Both plots consider RMS values ranging from 10 μV to 10 mV, which covers 1-100% an LSB for each curve. We note that Figs. 5-7 illustrate SNR of the amplitude but similar properties and utility are applicable for the phase. The phase has a bound of ± 5 dB tolerance based on simulations as opposed to the ± 2 dB for the amplitude.

It is worth mentioning an alternative simplified model that can be constructed from two points of view. First, one can construct the model directly considering the sampled signal $V_{\mathrm{ADC}}[k]$, assuming that the error terms $v_{\mathrm{n}}[k]$ and $q_{\mathrm{n}}[k]$ are independent of each other, the quantization error $q_n[k]$ is uniformly-distributed error over -LSB/2 to LSB/2, and $v_{\mathrm{n}}[k]$ is a normally distributed error with a variance of σ_n^2. Alternatively, one can arrive at this model by taking the DU model but allowing for continuous output values, as opposed to discrete LSB factors. We refer to this simplified model as the Continuous-Uniform (CU) model. The variance of the CU model is given by

$$\mathrm{var}(d_{\mathrm{n}}^{CU}) = LSB^2/12 + \sigma_S^2, \tag{23}$$

which was the modeling approach used in [15] for a similar problem. The SNR formulae for the CU model is equivalent to the DU model, i.e. (21) and (22), except one needs to substitute in (23) in place of $\mathrm{var}(d_{\mathrm{n}}^{DU})$. As a further connection between the CU and DU model, one could interpret the double integrals in (19) as the convolution of two pdfs, which is equivalent to the addition of two random variables, e.g.

$$P(d_{\mathrm{n}}^{DU} = m\mathrm{LSB}) = P\left(m - \frac{1}{2} < \frac{d_{\mathrm{n}}^{CU}}{\mathrm{LSB}} < m + \frac{1}{2}\right). \tag{24}$$

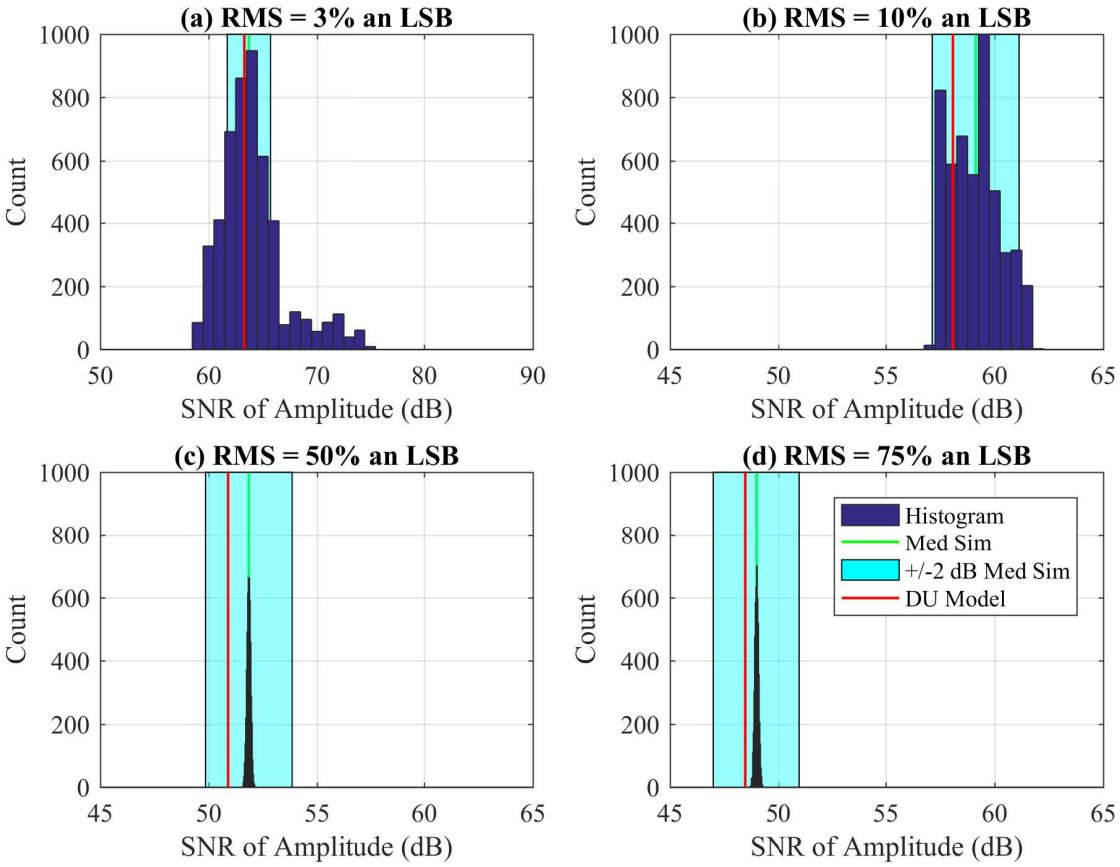

Fig. 6. Illustration of the distribution of the amplitude SNR for RMS values of 3%, 10%, 50%, and 75% of an LSB. The DU model falls within +/-2 dB of the median (Med) SNR. The distributions were constructed from 5,000 SNR values calculated from simulated (Sim) noisy signals with phase values uniformly ranging from 0 to 90 degrees. The input signal assumes the same scenario as the measured scenario (Fig. 4).

Figs. 4 and 5 shows the predicted SNR values using this model compared to the measurement data and a large set of simulated data and the DU model, respectively. Based on the simulation results, the CU model is expected to fall within 6.5 dB and 11 dB of the median SNR measurements of signal amplitude and phase, respectively. More specifically, the CU model is very accurate for high levels of noise, but substantially underestimates the SNR for lower levels of noise. For instance, the differences between the CU model and the mean simulated SNR amplitude values are less than 0.16 dB for RMS values $\geq$20% an LSB, and the maximum difference for RMS values $<$ 20% an LSB is 6.3 dB. In contrast, the analytic model and the DU model developed are accurate across all levels of noise (see Fig. 4). Quantitatively the difference between simulated data and the analytic model is less than 0.25 dB across all RMS values considered, and for the DU model the differences between the simulated mean and DU model from Fig. 5 are less than 1.35 dB over all RMS values considered. However, we note that if one is interested in larger % LSB RMS values (say greater than 20%), then the CU model may be desirable to use because of its added simplicity and its better accuracy in this error region. The CU model is more accurate than the DU model for RMS values greater than 20% an LSB (Fig. 4) because at these noise levels it is more accurate to assume that the AWGN is independent of the ADC noise (CU model) than to consider discrete mLSB-valued noise (DU-model). Further, in the low RMS region ($<$ 20% an LSB) the DU model is more accurate, which implies the discrete mLSB-valued noise is a better assumption. We note the region of low RMS (thermal) noise is important for applications that use low- to moderate-resolution ADCs, since these are not thermal noise limited [22].

VI. Conclusion

In conclusion this study has derived an analytical model to accurately describe the SNR of the amplitude and phase of an EIT measurement that considers both quantization caused by the ADC and additive system noise (prior to the ADC) that was not previously described in EIT literature. The analytical model (and our simulation code) was validated by a set of measured data. Furthermore, a practical model (DU model) was developed that a circuit designer could use as a tool to translate a target SNR to circuit-level specifications. The models developed here are being used in the design and development of analog readout front ends for an EIT system. Use of these tools within this design process will be reported.

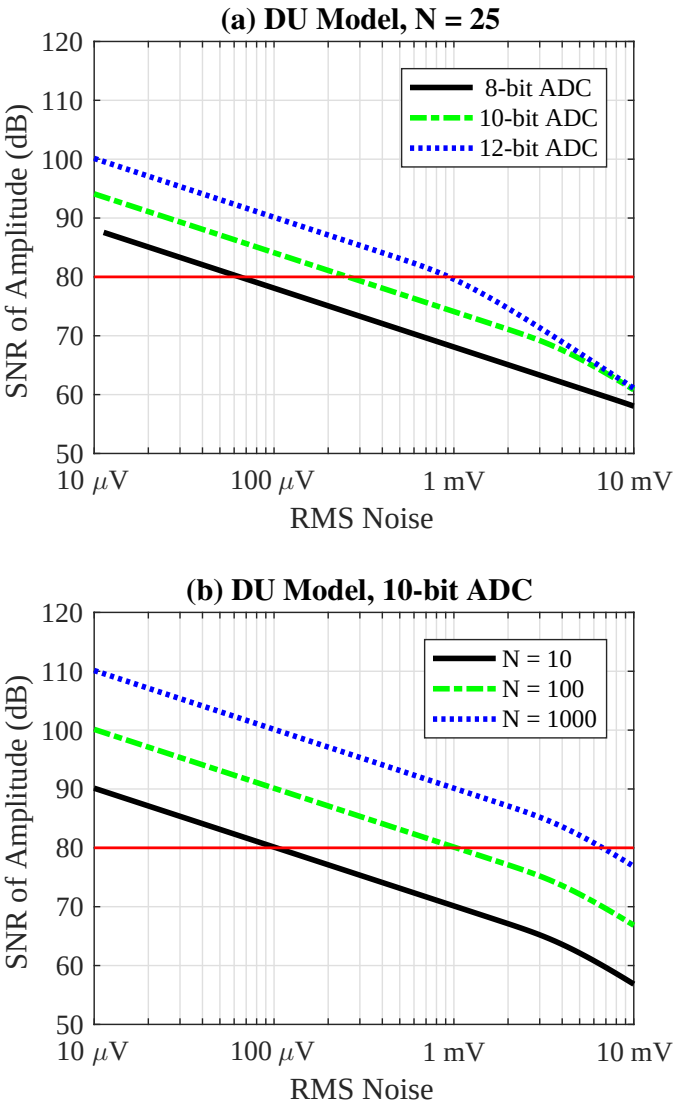

Fig. 7. Different combinations of circuit-level design choices that will achieve a measurement precision of 80 dB SNR. (a) A 10-bit ADC, followed by a 25-tap matched filter, can meet the 80 dB SNR specification as long as the total circuit noise (input-referred to the ADC) is 300 $\mu V_{\rm rms}$ or less. With the same 25-tap matched filter, a 12 bit ADC design can tolerate up to 1 $mV_{\rm rms}$ of noise and still meet the SNR target. (b) The number of taps in the matched filter can be traded off with the amount of circuit noise in order to achieve a desired SNR target. In this example with a 10 bit ADC, a system with a 10 tap filter would require a total noise level(input-referred to the ADC) of 100 $\mu V_{\rm rms}$ or less in order to achieve 80 dB SNR. Increasing the number of filter taps (and hence ADC sampling rate) by a factor of 100 will relax the noise specification to 6 $mV_{\rm rms}$.

Appendix A
Detailed Derivation of (7)

Assume that $ADC(\cdot)$ is a function denoting the ADC process. The output of the ADC is given by

$$V_{ADC}[k] = ADC(V_{BND}[k] + v_n[k]). \tag{A.1}$$

The deterministic error is defined as the difference between the ADC output of the noise-free input ($V^*_{ADC}[k] = ADC(V_{BND}[k])$) and the noise-free input, i.e.

$$q[k] = V^*_{ADC}[k] - V_{BND}[k]. \tag{A.2}$$

The probabilistic error is defined as the difference between the ADC output of the noisy signal and the ADC output of the noise-free signal, i.e.

$$d_n[k] = V_{ADC}[k] - V^*_{ADC}[k]. \tag{A.3}$$

A simple check can verify that (A.1) is equal to $V_{BND}[k]$ plus (A.2) and (A.3), which verifies and explicitly defines each term in (7).

Appendix B
Derivation of Variance of Amplitude

The amplitude is given in terms of the in-phase and quadrature component of the signal, i.e. (4). Thus we are interested in determining the following

$$var(A) = var\left(\sqrt{V_I^2 + V_Q^2}\right). \tag{A.4}$$

In order to derive the variance of the amplitude, (A.4), we use two linear approximations. The first is used to approximate V_I^2 and V_Q^2, and the second is used to approximate the square root function. The linearization of $y = x^2$ centered at the point a is given by

$$y(a + \Delta x) \approx a^2 + 2a\Delta x. \tag{A.5}$$

In terms of V_I the approximation is given by

$$V_I^2 = (\bar{V}_I + e_{VI})^2 \approx \bar{V}_I^2 + 2\bar{V}_I e_{VI}, \tag{A.6}$$

where the bar represents the mean of the in-phase component, and e_{VI} is the error associated with V_I. One can obtain a similar approximation for the V_Q component. Putting the approximations for V_I^2 and V_Q^2 together one has the following

$$V_I^2 + V_Q^2 \approx \bar{V}_I^2 + \bar{V}_Q^2 + 2(\bar{V}_I e_{VI} + \bar{V}_Q e_{VQ}). \tag{A.7}$$

Next, a linear approximation to the square root function is used, centered at the point $a = \bar{V}_I^2 + \bar{V}_Q^2$. The general form of the approximation is given by

$$y(a + \Delta x) \approx \sqrt{a} + \frac{1}{2\sqrt{a}}\Delta x. \tag{A.8}$$

In our application $\Delta x = 2(\bar{V}_I e_{VI} + \bar{V}_Q e_{VQ})$. Thus inserting our specific forms of a and Δx into (A.8) we have

$$\sqrt{V_I^2 + V_Q^2} \approx \sqrt{\bar{V}_I^2 + \bar{V}_Q^2} + \frac{2(\bar{V}_I e_{VI} + \bar{V}_Q e_{VQ})}{2\sqrt{\bar{V}_I^2 + \bar{V}_Q^2}}. \tag{A.9}$$

One can now return to (A.4) by taking the variance of both sides of (A.9), i.e.

$$var(A) = var\left(\sqrt{V_I^2 + V_Q^2}\right) \approx var\left(\frac{\bar{V}_I e_{VI} + \bar{V}_Q e_{VQ}}{\sqrt{\bar{V}_I^2 + \bar{V}_Q^2}}\right). \tag{A.10}$$

Next by using standard identities we have

$$var(A) \approx \frac{\bar{V}_I^2 var(V_I) + \bar{V}_Q^2 var(V_Q) + 2\bar{V}_I\bar{V}_Q cov(V_I, V_Q)}{\bar{V}_I^2 + \bar{V}_Q^2}, \tag{A.11}$$

where we have assumed that $var(V_I) = var(e_{VI})$ and $var(V_Q) = var(e_{VQ})$. One can then use (2) and (3), which should be equivalent to the average V_I and V_Q values, to simplify (A.11) to our final expression for the variance of the amplitude, i.e. (15).

APPENDIX C
DERIVATION OF VARIANCE OF PHASE

The phase derivation follows in a similar fashion. In this case we use two linear approximations in order to estimate the following

$$\mathrm{var}(\phi) = \mathrm{var}\left(\arctan\left(\frac{V_\mathrm{Q}}{V_\mathrm{I}}\right)\right) \tag{A.12}$$

The first linear approximation is with regards to the ratio, $V_\mathrm{Q}/V_\mathrm{I}$, and the second is with regards to the inverse tangent function. We begin by taking a first order approximation of the function $y = 1/x$. In general, this approximation is given by

$$y(a + \Delta x) \approx \frac{1}{a} - \frac{1}{a^2}\Delta x. \tag{A.13}$$

In our case we have

$$\frac{\bar{V}_Q + e_{VQ}}{\bar{V}_I + e_{VI}} \approx \frac{\bar{V}_Q + e_{VQ}}{\bar{V}_I} - (\bar{V}_Q + e_{VQ})\frac{e_{VI}}{\left(\bar{V}_I\right)^2} \tag{A.14}$$

where e_{VI} and e_{VQ} are small errors with regard to the in-phase and quadrature components. We drop the second order term, i.e. $e_{VQ}e_{VI}/\bar{V}_I^2$. Next, using a linear approximation to the inverse tangent function, y = arctan(x), which can be written as

$$y(a + \Delta x) \approx arctan(a) + \frac{1}{1 + a^2}\Delta x. \tag{A.15}$$

Assuming that $a = \bar{V}_Q/\bar{V}_I$, we have that

$$\arctan\left(\frac{V_Q}{V_I}\right) \approx \arctan\left(\frac{\bar{V}_Q}{\bar{V}_I}\right) + \frac{\Delta x}{1 + \left(\bar{V}_Q/\bar{V}_I\right)^2}. \tag{A.16}$$

Noting that $\Delta x = e_{VQ}/\bar{V}_I - e_{VI}\bar{V}_Q/\bar{V}_I^2$, we can use (A.16) to approximate (A.12) by the following

$$\mathrm{var}(\phi) \approx \mathrm{var}\left(\frac{\left(\frac{e_{VQ}}{\bar{V}_I} - \frac{e_{VI}\bar{V}_Q}{\bar{V}_I^2}\right)}{1 + \left(\bar{V}_Q/\bar{V}_I\right)^2}\right). \tag{A.17}$$

Pulling out the denominator from the variance, $var(aX) = a^2 var(X)$, and performing some simple manipulation of terms gives us

$$\begin{aligned}\mathrm{var}(\phi) \approx \quad & \left(\frac{\bar{V}_I^2}{\bar{V}_I^2+\bar{V}_Q^2}\right)^2 \mathrm{var}\left(\frac{e_{VQ}}{\bar{V}_I} - \frac{e_{VI}\bar{V}_Q}{\bar{V}_I^2}\right), \\ & \frac{1}{\left(\bar{V}_I^2+\bar{V}_Q^2\right)^2}\mathrm{var}\left(e_{VQ}\bar{V}_I - e_{VI}\bar{V}_Q\right).\end{aligned} \tag{A.18}$$

Further simplification yields the following

$$\begin{aligned}\mathrm{var}(\phi) \approx \quad & \frac{1}{\left(\bar{V}_I^2+\bar{V}_Q^2\right)^2}\left[\bar{V}_I^2\mathrm{var}(V_\mathrm{Q}) + \bar{V}_Q^2\mathrm{var}(V_\mathrm{I})\right. \\ & \left.-2\bar{V}_I\bar{V}_Q cov(V_\mathrm{I}, V_\mathrm{Q})\right].\end{aligned} \tag{A.19}$$

Similar to the amplitude variance calculation, we can then use (2) and (3) to simplify (A.19) to our final expression for the variance of the phase, i.e. (16).

APPENDIX D
COVARIANCE CALCULATION

First note the standard definition of the covariance,

$$cov(V_I, V_Q) = \mathrm{E}[V_I V_Q] - \mathrm{E}[V_I]\mathrm{E}[V_Q]. \tag{A.20}$$

The independent expectations of the in-phase and quadrature components, i.e. $E[V_I]$ and $E[V_Q]$, can be computed using similar equations to (13) and (14), which follows from the standard formula for the expectation from a discrete probability distribution, i.e.

$$\mathrm{E}[V_I] = \frac{2}{N}\sum_{k=0}^{N-1}\mathrm{E}\left[d_n[k]\right] sin\left(\frac{2\pi fk}{F_S}\right) \tag{A.21}$$

where each $\mathrm{E}\left[d_n[k]\right]$ can be calculated by the following

$$\mathrm{E}\left[d_n[k]\right] = \sum_{m=-\infty}^{\infty}\mathrm{P}(d_n[k] = mLSB)mLSB. \tag{A.22}$$

The joint expectation, $\mathrm{E}[V_I V_Q]$ is calculated by the following

$$\begin{aligned}\mathrm{E}[V_\mathrm{I}V_\mathrm{Q}] = \quad & \mathrm{E}\left[\left(\tfrac{2}{N}\textstyle\sum_{k=0}^{N-1} d_n[k]sin\left[\tfrac{2\pi fk}{F_S}\right]\right)\times\right. \\ & \left.\left(\tfrac{2}{N}\textstyle\sum_{m=0}^{N-1} d_n[m]cos\left[\tfrac{2\pi fm}{F_S}\right]\right)\right]\end{aligned} \tag{A.23}$$

which can be simplified to

$$\mathrm{E}[V_I V_Q] = \frac{4}{N^2}\sum_{k,m=0}^{N-1}\mathrm{E}\left[d_n[k]d_n[m]\right] sin\left[\frac{2\pi fk}{F_S}\right] cos\left[\frac{2\pi fm}{F_S}\right] \tag{A.24}$$

If k and m are different, then the errors should be independent and one can say that

$$\mathrm{E}\left[d_n[k]d_n[m]\right] = \mathrm{E}\left[d_n[k]\right]\mathrm{E}\left[d_n[m]\right]. \tag{A.25}$$

Each of the $\mathrm{E}\left[d_n[k]\right]$ can be calculated using (A.22). If k and m are the same then we need to calculate $\mathrm{E}\left[(d_n[k])^2\right]$, which was essentially already calculated in (8).

ACKNOWLEDGMENT

This work was supported in part by the U.S. National Institutes of Health under Grant 5R01CA143020, National Science Foundation under Grant No. 1418497, and US DoD CDMRP Grant W81XWH-15-1-0571.

The authors would also like to enumerate individual authors contributions. These contributions are as follows: Murphy developed the analytic and DU models and drafted the paper, Takhti worked on mathematical modeling/simulation including the deriving the CU model, and designed the measurement device, Skinner assembled hardware, performed measurements, and contributed to resolving phase drift issues, and Halter and Odame directed the research and provided important editorial and technical insights.

REFERENCES

[1] R.H. Bayford, "Bioimpedance tomography (electrical impedance tomography)," Annual Rev. Biomed. Eng., vol. 8, pp. 63-91, 2006.

[2] S.H. Arshad, , Jordan S. Kunzika, Ethan K. Murphy, Kofi Odame, Ryan J. Halter, "Towards a Smart Phone-Based Cardiac Monitoring Device using Electrical Impedance Tomography," IEEE BioCAS conference proceedings, Oct. 22-24, 2015.

[3] D. Holder, Electrical Impedance Tomography Institute of Physics Publishing, Bristol, 2005.

[4] Holder, David S. "Electrical impedance tomography of brain function." Automation Congress, 2008. WAC 2008. World. IEEE, 2008.

[5] A. Adler, et al., "Whither lung EIT: Where are we, where do we want to go and what do we need to get there?" Physiol. Meas., vol. 33, pp. 679-694, 2012.

[6] R.J. Halter, A. Hartov, and K.D. Paulsen, "A broadband high-frequency electrical impedance tomography system for breast imaging," Biomedical Engineering, IEEE Trans., vol. 55, no. 2, pp. 650-659, 2008.

[7] R.W.M. Smith, I.L. Freeston, B.H. Brown, and A. M. Sinton, "Design of a phase-sensitive detector to maximize signal-to-noise ratio in the presence of Gaussian wideband noise," Meas. Sci. Technol., vol. 3, pp.1054-1062, 1992.

[8] N. Liu, G.J. Saulnier, J.C. Newell, "A Multichannel Synthesizer and Voltmeter for Electrical Impedance Tomography," Proc. 25th Annual International Conf. of IEEE EMBS, Cancun, Mexico, Sept. 17-21, 2003.

[9] Liu, Ning, "ACT4: A high-precision, multi-frequency electrical impedance tomograph," Ph.D. Dissertation, Rensselaer Polytechnic Institute, 2007.

[10] Saulnier G, "Hardware" In Holder D, "Electrical Impedance Tomograph," Institute of Physics Publishing, Bristol, 2005.

[11] S. Kahn, P. Manwaring, A. Borsic, R.J. Hlater, "FPGA-based voltage and current dual drive system for high frame rate electrical impedance tomography," Medical Imaging, IEEE Trans., vol. 34, no. 4, pp. 888-901, 2015.

[12] H. Wi, H. Sohal, A. L. McEwan, E. J. Woo, and T. I. Oh, "Multi-frequency electrical impedance tomography system with automatic self-calibration for long-term monitoring," IEEE Trans. Biomed. Circuits Syst., vol. 8, no. 1, pp. 119128, 2014.

[13] A.G. Clavier, P.F. Panter, and D.D. Grieg, "Distortion in a pulse count modulation system," Trans. on the American Institute of Electrical Engineers, vol 66, no. 1, pp. 989-1005, 1947.

[14] W.R. Bennett, "Spectra of quantized signals," Bell System Technical Journal, vol. 27, no. 3, pp. 446-472, 1948.

[15] R.A. Wannamaker, S.P. Lipshitz, J. Vanderkooy, and J.N. Wright, "A theory of nonsubtractive dither," Signal Processing, IEEE Transactions on, vol. 48, no. 2, pp. 499-516, 2000.

[16] G.L. Turin, "An introduction to digitial matched filters," Proceedings of the IEEE, vol. 64, no. 7, pp. 1092-1112, 1976.

[17] W.Sansen, Analog Design Essentials, 2006, Springer.

[18] P.Lee, "Low Noise Amplifier Selection Guide for Optimal Noise Performance," Analog Devices, Application Note 940, 2009.

[19] P.R. Gray, et al., "Analysis and design of analog integrated circuits," Wiley, 2001.

[20] D.A. Johns and K. Martin, "Analog integrated circuit design," John Wiley & Sons, 2008.

[21] S.M. Ross, "Introduction to Probability Models," Academic Press, San Diego, CA, 2000.

[22] B. Murmann, "Energy Limits in A/D Converters," Faible Tension Faible Consommation (FTFC), 2013 IEEE, 2013.

Ethan Murphy is a Research Associate at Thayer School of Engineering at Dartmouth College. He received his BS and MS from Worcester Polytechnic Institute in 2002 and PhD from Colorado State University in 2007 in mathematics. He has worked in industrial and academic positions since coming to Dartmouth in 2014. His interests are in inverse problems, especially EIT, medical imaging, data fusion, and error analysis.

Mohammad Takhti (S09) received his B.S. degree in electrical engineering from the University of Dezful in Dezful, Iran, and his M.S. degree in electrical engineering from the K. N. Toosi University of Technology (KNTU), in Tehran, Iran.

He worked in the Research Laboratory for Integrated Circuits and Systems (ICAS) at KNTU as a Research Assistant from 2007 to 2010 and as an Associate Researcher from 2010 to 2013.

He is currently pursuing his Ph.D. degree in electrical engineering at the Thayer School of Engineering at Dartmouth College, Hanover, NH, USA. His research interests include low-power analog and mixed-mode IC design for biomedical wearable and portable applications.

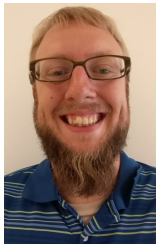

Joseph Skinner (BS07) is a Research Engineer at the Thayer School of Engineering at Dartmouth College. Joe's primary interest is in hardware level integrated circuit layout and design. This work is most frequently applied to low power medical sensing devices in addition to other sampling systems used in medical settings.

Ryan Halter (M04) is an Assistant Professor of Biomedical Engineering at the Thayer School of Engineering at Dartmouth College. His research interests are in the fields of medical device development and medical imaging. He primarily focuses on exploring the use of electrical impedance spectroscopy and tomography in clinical applications including cancer detection and imaging, surgical margin assessment, and cardiac imaging.

Kofi Odame (S06M08-SM'15) is an Associate Professor of Electrical Engineering at the Thayer School of Engineering at Dartmouth College. Kofi's primary interest is in analog integrated circuits for nonlinear signal processing. This work has applications in low-power electronics for implantable and wearable biomedical devices, as well as in autonomous sensor systems.